PROCEEDINGS OF SPIE

SPIEDigitalLibrary.org/conference-proceedings-of-spie

Harmonic holography for three-dimensional cellular imaging

Chia-Lung Hsieh, Rachel Grange, Ye Pu, Demetri Psaltis

Chia-Lung Hsieh, Rachel Grange, Ye Pu, Demetri Psaltis, "Harmonic holography for three-dimensional cellular imaging," Proc. SPIE 7329, Three-Dimensional Imaging, Visualization, and Display 2009, 73290H (6 May 2009); doi: 10.1117/12.820801

SPIE.

Event: SPIE Defense, Security, and Sensing, 2009, Orlando, Florida, United States

Harmonic holography for three-dimensional cellular imaging

Chia-Lung Hsieh[a,b], Rachel Grange[a], Ye Pu[a,b], Demetri Psaltis[*a,b]
[a] School of Engineering, EPFL, Station 17, 1015 Lausanne, Switzerland;
[b] Department of Electrical Engineering, California Institute of Technology, 1200 East California Boulevard, MC 136-93, Pasadena, California 91125, USA

ABSTRACT

Luminescent markers play a key role in imaging techniques for life sciences since they provide a contrast mechanism between signal and background. We describe a new type of marker using second harmonic generation (SHG) from noncentrosymmetric $BaTiO_3$ nanocrystals. These nanoparticles are attractive due to their stable, non-saturating and coherent signal with a femtosecond-scale response time and a broad flexibility in the choice of excitation wavelength. We use the coherent SHG signal from $BaTiO_3$ nanoparticles for three-dimensional (3D) imaging without scanning. We built a harmonic holographic (H^2) microscope which records digital holograms at the second harmonic frequency. High-resolution 3D distributions of these SHG markers in mammalian cells are successfully captured and interpreted by the H^2 microscope.

Keywords: second harmonic generation, barium titanate, nanoparticle, digital holography, biological cells, three-dimensional microscopy

1. INTRODUCTION

At micro- and nanometer scale, the processes of life involve fast dynamics of complex 3D structures. Visualizing these processes often requires a technique to image in four dimensions with sufficient spatio-temporal resolution over a long period of time. Holography is a natural choice because of its capability to capture 3D images without the need for scanning. However, conventional holography lacks the capability of discrimination between signal and background, a fundamental requirement in modern microscopy. Here we present a H^2 microscopy system using SHG from noncentrosymmetric $BaTiO_3$ nanoparticles as a contrast mechanism. We refer to these nanoparticles as "Second Harmonic Radiation IMaging Probes (SHRIMPs)". Fluorescent bio-markers such as organic dyes [1], green fluorescent protein (GFP) [2], and quantum dots (QDs) [3] have been popularly used for biomedical imaging due to their outstanding brightness and biocompatibility [4, 5]. Due to the intrinsic properties of SHG, SHRIMPs emit a stable coherent signal which is suitable for long-term observations. These types of observations are usually complicated when using the fluorescent signal because of photobleaching and luminescence blinking [6, 7].

When a nanocrystal of noncentrosymmetric structure is optically excited at a fundamental frequency, it emits the optical signal at the exact doubled frequency. Only materials with crystalline structures lacking a center of symmetry are capable of efficient SHG. As a result, when imaged at the second harmonic frequency, SHRIMPs provide an effective mechanism of contrast between the markers and the generally unstructured or isotropic biological microenvironment. Ordered and highly polarizable biological noncentrosymmetric structures, such as the collagen fibers, have been known for endogenous SHG [8]. However, in most of the biological cell components, the endogenous SHG from the cell interface layers is weak [9].

Compared to fluorescent markers, SHRIMPs allow for significantly better imaging modalities due to their intrinsic properties. Unlike fluorescence, the process of SHG only involves virtual electron energy transition without nonradiative energy loss. Owing to this lossless, virtual transition process, SHRIMPs do not bleach over time and emit a stable, non-saturating signal with a femtosecond-scale response time. This allows for the observation of fast dynamic processes over a long time. Furthermore, SHG is generally a non-resonant process which offers the flexibility in the choice of excitation wavelength. This also results in the flexibility of tuning the wavelength of the SHG signal by changing the excitation wavelength accordingly. The coherent nature of the SHG signal is also a main advantage, providing a possibility to detect the second harmonic signal with interferometric optical techniques [10-13].

*demetri.psaltis@epfl.ch; phone +41 21 693 7795; fax +41 21 693 6930; http://lo.epfl.ch

Three-Dimensional Imaging, Visualization, and Display 2009,
edited by Bahram Javidi, Jung-Young Son, Manuel Martinez-Corral, Fumio Okano, Wolfgang Osten,
Proc. of SPIE Vol. 7329, 73290H · © 2009 SPIE · CCC code: 0277-786X/09/$18 · doi: 10.1117/12.820801

The principle of harmonic holography was recently demonstrated [10]. When the digital hologram is recorded at the doubled frequency, it captures both the amplitude and phase information of the SHG object field. Therefore the 3D field distribution, reflecting the 3D distribution of the SHRIMPs could be recorded without scanning. The spatial resolution is limited by the diffraction of light at the half wavelength, and the temporal resolution is limited by the laser pulse duration. Several holographic techniques have been developed for bio-imaging, for example the linear and fluorescent holographic microscopy [14-16]. H^2 microscopy is especially suitable for long-term imaging with luminescent markers due to the high imaging contrast provided by detecting the signal at SHG frequency: the background signal (linear background scattering and autofluorescence) can be efficiently removed by optical filters.

The SHG properties of several kinds of nanocrystals have been recently reported: ZnO [17, 18], $Fe(IO_3)_3$ [19], $KNbO_3$ [20], $KTiOPO_4$ (KTP) [11, 21] and SHG-active crystalline organic-inorganic hybrid nanoparticles [22]. In this paper, we report H^2 bioimaging with $BaTiO_3$ nanoparticles as SHRIMPs. We demonstrate the H^2 microscopy where the 3D distribution of SHRIMPs inside artificial samples and mammalian cells was recorded and reconstructed by one digital hologram.

2. SECOND HARMONIC GENERATION FROM BARIUM TITANATE NANOPARTICLES

We worked with commercial 30 nm and 90 nm $BaTiO_3$ nanoparticles dry powder from Nanoamor and Techpowder respectively, whose tetragonal crystal structure is non-centrosymmetric and allowing for efficient SHG. Figure 1 shows the scanning electron microscope (SEM) images of 30 nm and 90 nm $BaTiO_3$ spherical nanoparticles.

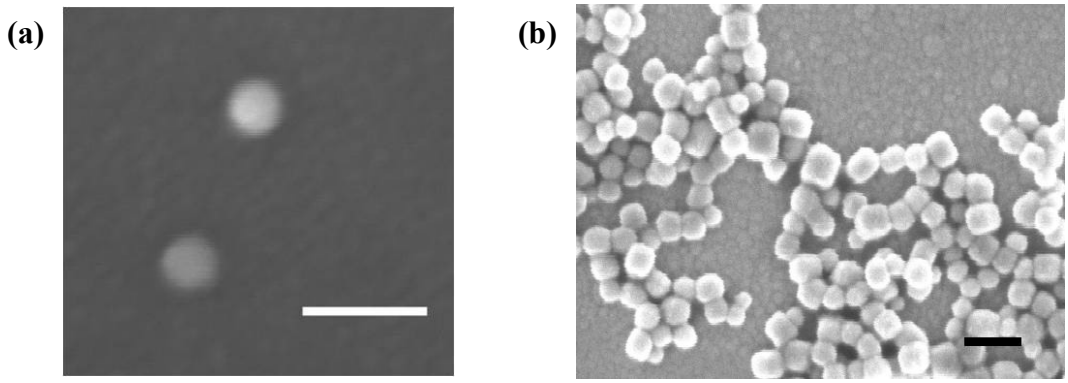

Fig. 1. The SEM images of $BaTiO_3$ spherical nanoparticles. (a) 30 nm $BaTiO_3$ nanoparticles. The scale bar is 100 nm. (b) 90 nm $BaTiO_3$ nanoparticles. The scale bar is 200 nm.

We characterized the SHG response of the nanoparticles which were deposited on a glass substrate. A Ti:sapphire oscillator beam of 800 nm wavelength, 2 nJ pulse energy, 100 fs pulse width, and 80 MHz repetition rate was used for excitation. The laser beam was focused to reach the peak excitation intensity of 1 GW/cm^2 on the sample. Figure 2 shows the second order nonlinear response of a ~500 nm $BaTiO_3$ cluster as a function of the excitation peak intensity up to 4 GW/cm^2 at the sample position, which exactly follows a quadratic law. The inset of Fig. 2 shows the SHG optical spectrum centered around 400 nm with a FWHM of 5 nm. We also recorded the SHG radiation over more than an hour without significant drop of the intensity.

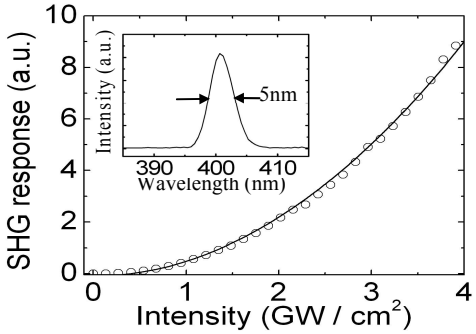

Fig. 2. Quadratic SHG response of $BaTiO_3$ nanoparticles versus the excitation peak intensity. The circles show the experimental results while the line is the quadratic fit. Inset: optical spectrum of the SHG signal.

We used a standard two-photon scanning confocal microscope (Leica, SP5) to image the 90 nm $BaTiO_3$ nanoparticles deposited on a glass substrate. The excitation laser was femtosecond laser pulses at 800 nm from a Ti:sapphire oscillator. Figure 3 shows the transmission image and the SHG image of the $BaTiO_3$ nanoparticles. In the transmission image, the nanoparticles scatter light so that they appear as dark spots. In the SHG image, the $BaTiO_3$ nanoparticles give great contrast. A good correspondence of the transmission image to the SHG image indicates the uniform capability of SHG from $BaTiO_3$ nanoparticles. The intensity of the SHG signal from the nanoparticles varies, which may be because of the variation in particle size and also the polarization dependent SHG response.

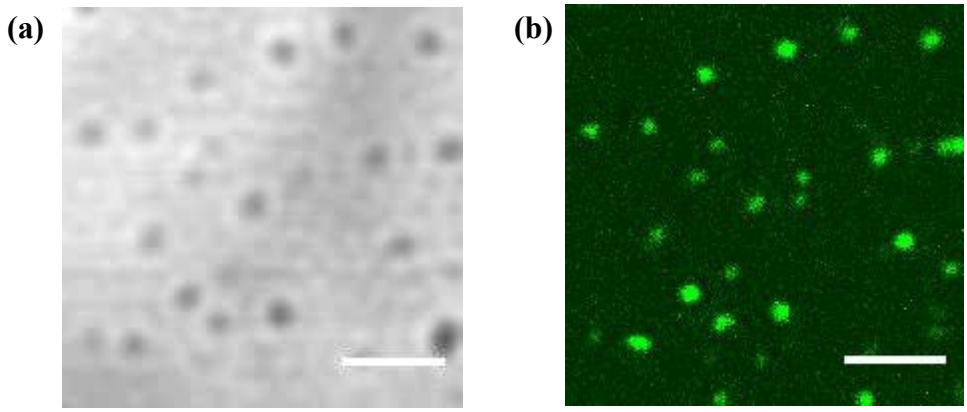

Fig. 3. Confocal images of $BaTiO_3$ nanoparticles deposited on a glass substrate. (a) Transmission image. (b) SHG image. The scale bars are 5 μm.

3. CELL IMAGING WITH SHRIMPS

We demonstrate the capability of SHRIMPs as biomarkers for cell imaging. The cultured mammalian (HeLa) cells were first stained with Calcein so that we could see the cell through two-photon fluorescence signal from the Calcein under the laser excitation. The cells were then fixed with 3.7% parafolmaldehyde in phosphate buffered saline (PBS) before being stained by SHRIMPs. Meanwhile, the 30 nm $BaTiO_3$ SHRIMPs were stabilized with aminomethylphosphonic acid. The fixed cells were incubated with SHRIMPs for 24 hours at 4 ^oC. We imaged the HeLa cells with SHRIMPs by a standard two-photon scanning confocal microscope (Leica, SP5) as mentioned above. The SHG signal from SHRIMPs and the two-photon fluorescent signal from Calcein were collected simultaneously by two separated channels. Figure 4 shows a confocal section image of the cells with SHRIMPs. The SHRIMPs absorbed non-specifically on the cell membrane due to the electrostatic force. SHG from SHRIMPs gives good contrast in cell imaging because the endogenous SHG from cell components and interfaces is weak [9].

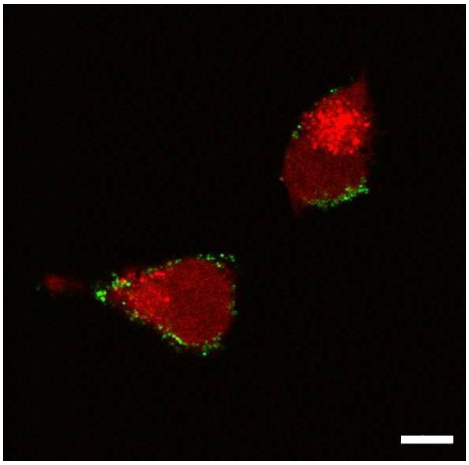

Fig. 4. Superimposed confocal section images of two calcein-stained HeLa cells with SHRIMPs non-specifically absorbed on them. Calcein emits two-photon fluorescence signal and shows the shape of a HeLa cell (shown in red). SHRIMPs absorbed on the cells emit SHG signal (shown in green). The scale bar is 10 μm.

4. H^2 MICROSCOPY

We built a H^2 microscope to demonstrate the potential of SHRIMPs for scan-free 3D imaging. The excitation light source consisted of 150 fs laser pulses centered at 800 nm wavelength (repetition rate 76 MHz) from a Ti:sapphire oscillator. The peak intensity of the excitation is 1.5 GW/cm^2, which is 100 times less than the cell damage threshold [23] and is also 100 times less than that used in Ref. 10. The experimental setup is shown in Fig. 5. The H^2 microscope can be understood as a 4F imaging system followed by a holographic recording system. The SHG signal from SHRIMPs was collected and optically magnified 80 times by a 4F system consisting of a 0.9 NA microscope objective and a lens of 20 cm focal length. The detector was an electron multiplying charge coupled device (EMCCD) camera. We put the EMCCD away from the 4F imaging plane so that the object field could propagate and fill the detection area of EMCCD. The hologram recording distance, i.e. the distance between the SHG image formed by the 4F system and the EMCCD, was 20 cm. A plane wave at doubled frequency generated by a separate β-barium borate (BBO) crystal served as the reference beam. The intensity ratio between the signal maximum and the reference beam is set to be 1:10. The signal and reference pulses were collinearly overlapping both spatially and temporally on the EMCCD, and as a result an on-axis digital hologram was recorded at the SHG wavelength. The digital reconstruction is discussed in details in Ref. 10. The inherent twin image has little effect on reconstructed image due to the long hologram recording distance.

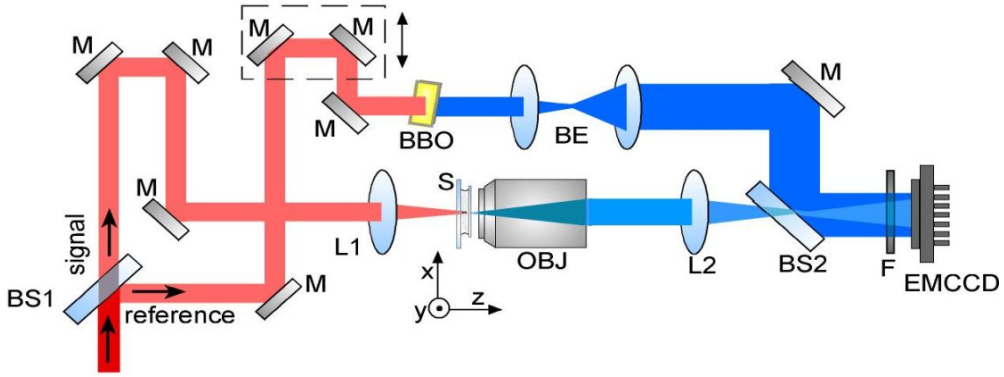

Fig. 5. H^2 microscope experimental setup. BS1 and BS2, beam splitters; M, mirror; L1 and L2, lens; S, sample; OBJ, microscope objective; BE, beam expander; F, band-pass filter centered at 400 nm. BS1 splits the laser into signal and reference beams. In the signal arm, L1 slightly focuses the excitation beam into the sample with SHRIMPs. OBJ and L2 form a 4F imaging system to collect and optically magnify the SHG image of SHRIMP. The EMCCD is placed away from the 4F imaging plane. A band-pass filter is placed in front of the EMCCD to remove the excitation from the SHG signal. The reference beam goes through a translation stage and a BBO crystal so that the coherent reference SHG laser pulses are generated and can be temporally and spatially overlapped with the signal on the EMCCD. The signal and reference beams are combined collinearly by BS2 and therefore an on-axis digital hologram is recorded on the EMCCD.

5. SINGLE SHRIMP DETECTION WITH THE H^2 MICROSCOPE

The H^2 microscope was sensitive enough to image an isolated $BaTiO_3$ nanocrystal. Since the particle size is smaller than the optical diffraction limit at the SHG wavelength, the image of the particle reflects the spatial resolution of the H^2 microscope. Figure 6 (a) shows the focused SHG image of an isolated $BaTiO_3$ nanocrystal taken by the conventional 4F imaging system. The spot size is 0.4 μm which is the diffraction limit. We then imaged the same nanocrystal with the H^2 microscope. The single nanocrystal behaved as a point source at the SHG frequency. The radiated spherical waves interfered with the reference plane waves and a set of interference rings (Fresnel zone plates) were formed and recorded on the detector plane. By digital propagation, we can reconstruct the field at any plane from the recorded Fresnel zone plates. Figure 6 (b) is the harmonic holographic reconstructed image of the same $BaTiO_3$ particle on the object plane, which shows the same spot size as the Fig. 6 (a). Therefore, the H^2 microscope has diffraction-limited resolution. The axial resolution of the H^2 microscope can be measured by digital holographic reconstruction of a stack of images along the axial direction. The measured axial resolution was about 2 μm as shown in Fig. 6 (c). The axial resolution may be improved by calibrating the aberration introduced by the optics for the signal collection, especially the spherical aberration introduced by the objective.

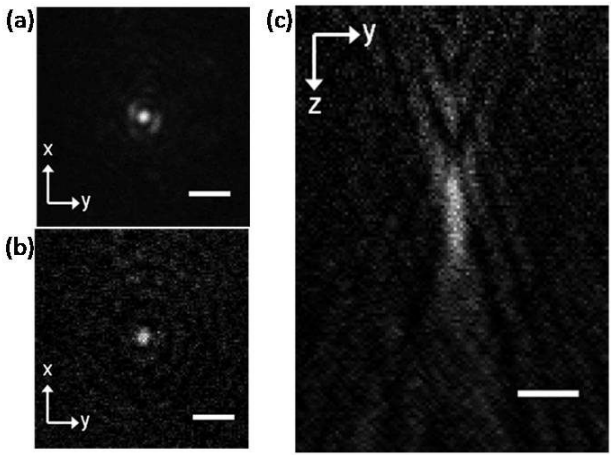

Fig. 6. Spatial resolution of the H^2 microscope measured by imaging an isolated $BaTiO_3$ particle. (a) SHG intensity image measured by a conventional microscope. (b) Holographic reconstructed intensity image at the object plane. (c) Cross section of a stack of holographic reconstructed intensity images along the axial direction. The scale bars are 2 μm.

6. H^2 MICROSCOPIC 3D IMAGING

The capability of the H^2 microscope for 3D SHRIMPs imaging was first evaluated by imaging an artificial 3D sample. We prepared a 3D distribution of SHRIMPs by randomly embedding 30-nm $BaTiO_3$ nanoparticles in a ~100 μm thick polydimethylsiloxane (PDMS) film. The SHRIMPs were immobilized inside the film when the PDMS was cured. Figure 7 (a)-(d) show the conventional SHG microscope images of four sub-micron $BaTiO_3$ clusters on four different planes under excitation. These four clusters were then imaged by the H^2 microscope. The results are shown in Fig. 7 (e)-(h). We changed the focus by digitally reconstructing the images at different planes. The relative depths of the reconstructed planes were 0, 9.4, 17.2, and 20.3 μm respectively. The reconstructed images in Fig. 7 (e)-(h) agree well with the SHG images in Fig. 7 (a)-(d), suggesting that 3D distributions of SHRIMPs can be reliably recorded and interpreted from a single digital hologram without scanning. It is worth noting that the H^2 microscopy would have difficulty imaging a high density of SHRIMPs [24]. This difficulty results from the intrinsic speckle noise and it is a fundamental limit of storing 3D information with a 2D image. However, when the density of SHRIMPs is low, the H^2 microscopy with SHRIMPs makes scan-free 3D imaging possible.

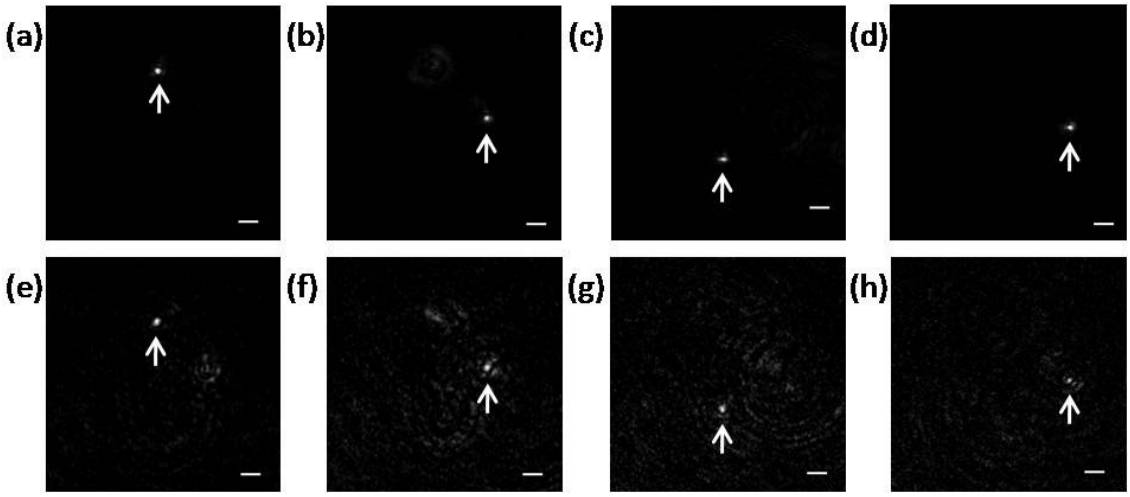

Fig. 7. Images of SHRIMPs embedded in PDMS. (a)-(d): SHG images of SHRIMPs on four different planes, focusing by moving the optics with a conventional microscope. (e)-(h): Holographic reconstructed images of SHRIMPs on four corresponding planes, focusing by digital reconstruction. The relative depths of these four planes are 0, 9.4, 17.2, and 20.3 μm respectively. Scale bars are 2 μm.

7. 3D IMAGING OF THE SHRIMPS IN MAMMALIAN CELLS

SHRIMPs make scan-free 3D bio-imaging possible when they are labeled on the targets of interest and imaged with the H^2 microscope. Here we demonstrate the capability of the H^2 microscopy with SHRIMPs for 3D bio-imaging, as well as the biocompatibility of $BaTiO_3$ nanoparticles as SHRIMPs. The sample under analysis was mammalian (HeLa) cells non-specifically labeled with SHRIMPs. HeLa cells were incubated for 24 hours at 37 ^oC with 30-nm $BaTiO_3$ particles that have been stabilized with aminomethylphosphonic acid. During the incubation, the amine group present on the SHRIMPs surface encouraged the cells to uptake them through endocytosis [25]. SHRIMPs would be engulfed non-specifically into vesicles and packed as clusters randomly by the cells. In this way a 3D distribution of SHRIMPs was formed inside the cells. After 24-hour incubation, the HeLa cells were still alive. We washed away the unbound SHRIMPs with a buffer solution (phosphate buffered saline, PBS) and fixed the cells with 3.7% parafolmaldehyde. The sample was then ready to be holographically imaged. Figure 8 (a) shows the bright field transmission image of a cell under analysis. When the cell was under excitation of the laser, SHRIMPs inside it emitted SHG signals. Figure 8 (b) shows the SHG image of SHRIMPs taken by a conventional microscope. In Fig. 8 (b), we observe some SHRIMPs appear as bright spots because they are on focus, while the others are not visible because they are out of focus. The SHRIMPs are numbered for ease of discussion. Figure 8 (c) shows the superposition of the bright field transmission image of the cell and the SHG signal from SHRIMPs, showing that the SHRIMPs non-specifically labeled the cells. We imaged the same area with the H^2 microscope. By digital reconstruction, we observe several SHRIMPs get on focus at different planes. Figure 8 (d)-(f) show the reconstructed images on three relative depths of the cell (0, 3.12, and 6.24 μm) where different clusters get on focus respectively. Since the cells uptook the SHRIMPs randomly, the size of the SHRIMP clusters, and therefore the SHG intensity, varied in a wide range. Figure 8 (g) shows the normalized line intensity profiles of the six clusters under analysis when they are on focus through digital reconstruction. All of them show a high signal to noise ratio. The cluster number 3 has a weak signal and in its line intensity profile we can see the defocused signal from the cluster number 4.

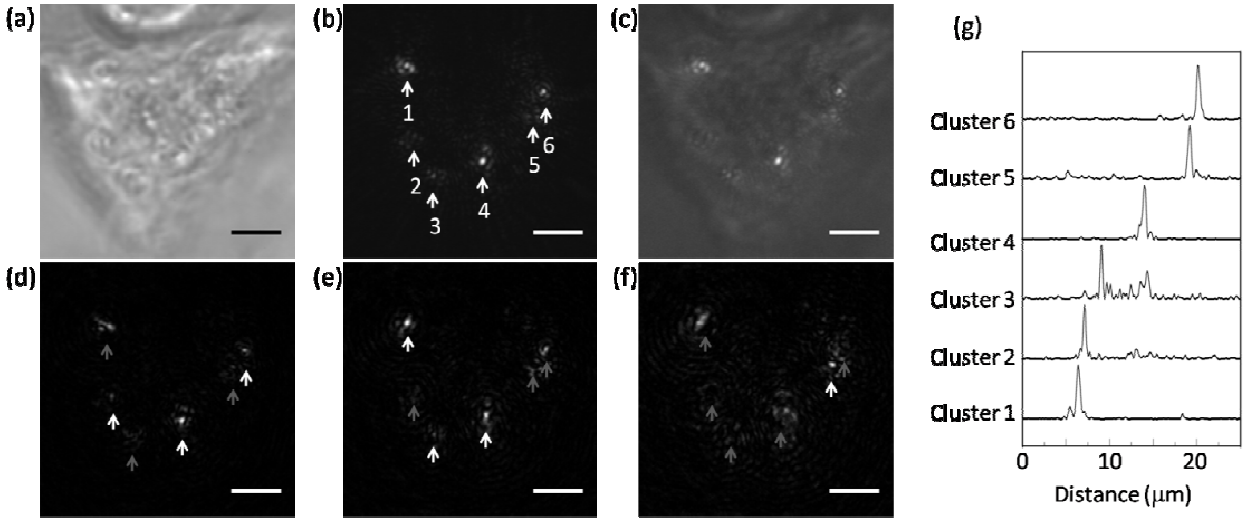

Fig. 8. H^2 microscope 3D imaging of SHRIMPs non-specifically labeling the HeLa cells (a) Bright field transmission image of the HeLa cell under analysis. (b) The SHG image of SHRIMPs taken by a conventional microscope. Six SHRIMPs clusters were under analysis. Some of them cannot be seen clearly because they are out of focus. (c) The superposition image of (a) and (b), showing that the cells uptook the SHRIMPs. (d)-(f) H^2 reconstructed images at three different planes (relative depths of 0, 3.12 and 6.24 μm respectively). The white arrows show the SHRIMPs that are on focus, while the gray arrows show the SHRIMPs that are out of focus. The SHRIMP labeled with number 4 is a big cluster, so it is on focus both in (d) and (e). The scale bars are 5 μm. (g) Normalized line intensity profiles of the six clusters when they are on focus.

The acquisition time of the digital hologram was 1 minute, limited by the integration time for detectable signal. The acquisition time can be further optimized by increasing the excitation power and also the sensitivity of the detection. The

peak intensity used in the experiment was 100 times weaker than the critical intensity affecting the cellular metabolism [23], so there is a room to further increase the pump intensity, and, as a result, the SHG signal intensity. The collection efficiency of the SHG signal was ~1%, which could also be significantly improved by adapting the optics for the SHG frequency. Moreover, the reference beam in holography can serve as a coherent local oscillator, leading to a gain in signal to noise ratio and a shot noise-limited performance of detection even at fast read-out [10]. As a pulsed holographic technique, the H^2 microscopy could reach a temporal resolution limited by the laser pulse width [10, 26].

8. CONCLUSION

We demonstrate the use of $BaTiO_3$ nanoparticles as SHRIMPs for bio-imaging. We built a H^2 microscopy with $BaTiO_3$ nanoparticles as SHRIMPs for high-resolution 3D imaging. 3D distributions of SHRIMPs in artificial structures and HeLa cells are recorded and interpreted with diffraction-limited resolution by a digital hologram without scanning.

REFERENCES

[1] Griffin, B. A., Adams, S. R., and Tsien, R. Y., "Specific covalent labeling of recombinant protein molecules inside live cells," Science 281, 269-272 (1998).

[2] Chalfie, M., Tu, Y., Euskirchen, G., Ward, W. W., and Prasher, D. C.,"Green fluorescent protein as a marker for gene-expression," Science 263, 802-805 (1994).

[3] Chan, W. C. W., and Nie, S. M., "Quantum dot bioconjugates for ultrasensitive nonisotopic detection," Science 281, 2016-2018 (1998).

[4] Miyawaki, A., Sawano, A., and Kogure, T., "Lighting up cells: labelling proteins with fluorophores," Nature Cell Biol. 5, S1-S7 (2003).

[5] Giepmans, B. N. G., Adams, S. R., Ellisman, M. H., and Tsien, R. Y., "Review - The fluorescent toolbox for assessing protein location and function," Science 312, 217-224 (2006).

[6] Dickson, R. M., Cubitt, A. B., Tsien, R. Y., and Moerner, W. E., "On/off blinking and switching behaviour of single molecules of green fluorescent protein," Nature 388, 355-358 (1997).

[7] Patterson, G. H., and Piston, D. W., "Photobleaching in two-photon excitation microscopy," Biophys. J. 78, 2159-2162 (2000).

[8] Campagnola, P. J., and Loew, L. M., "Second-harmonic imaging microscopy for visualizing biomolecular arrays in cells, tissues and organisms," Nat Biotech 21, 1356-1360 (2003).

[9] Campagnola, P. J., Wei, M. D., Lewis, A., and Loew, L. M., "High-resolution nonlinear optical imaging of live cells by second harmonic generation," Biophys. J. 77, 3341-3349 (1999).

[10] Pu, Y., Centurion, M., and Psaltis, D., "Harmonic holography: a new holographic principle," Appl. Opt. 47, A103-A110 (2008).

[11] Xuan, L. L., Brasselet, S., Treussart, F., Roch, J. F., Marquier, F., Chauvat, D., Perruchas, S., Tard, C., and Gacoin, T., "Balanced homodyne detection of second-harmonic generation from isolated subwavelength emitters," Appl. Phys. Lett. 89, 121118 (2006).

[12] Chen, J., Machida, S., and Yamamoto, Y., "Simultaneous measurement of amplitude and phase in surface second-harmonic generation," Opt. Lett. 23, 676-678 (1998).

[13] Kluge, S., Budde, F., Dohnke, I., Rechsteiner, P., and Hulliger, J., "Phase-sensitive second-harmonic microscopy reveals polarity of topologically centrosymmetric molecular crystals," Appl. Phys. Lett. 81, 247-249 (2002).

[14] Marquet, P., Rappaz, B., Magistretti, P. J., Cuche, E., Emery, Y., Colomb, T., and Depeursinge, C., "Digital holographic microscopy: a noninvasive contrast imaging technique allowing quantitative visualization of living cells with subwavelength axial accuracy," Opt. Lett. 30, 468-470 (2005).

[15] Schilling, B. W., Poon, T. C., Indebetouw, G., Storrie, B., Shinoda, K., Suzuki, Y., and Wu, M. H., "Three-dimensional holographic fluorescence microscopy," Opt. Lett. 22, 1506-1508 (1997).

[16] Rosen, J., and Brooker, G., "Non-scanning motionless fluorescence three-dimensional holographic microscopy," Nat. Photonics 2, 190-195 (2008).

[17] Kachynski, A. V., Kuzmin, A. N., Nyk, M., Roy, I., and Prasad, P. N., "Zinc oxide nanocrystals for nonresonant nonlinear optical microscopy in biology and medicine," J. Phys. Chem. C 112, 10721-10724 (2008).

[18] Johnson, J. C., Yan, H. Q., Schaller, R. D., Petersen, P. B., Yang, P. D., and Saykally, R. J., "Near-field imaging of nonlinear optical mixing in single zinc oxide nanowires," Nano Letters 2, 279-283 (2002).
[19] Bonacina, L., Mugnier, Y., Courvoisier, F., Le Dantec, R., Extermann, J., Lambert, Y., Boutou, V., Galez, C., and Wolf, J. P., "Polar Fe(IO3)(3) nanocrystals as local probes for nonlinear microscopy," Appl. Phys. B-Lasers and Optics 87, 399-403 (2007).
[20] Nakayama, Y., Pauzauskie, P. J., Radenovic, A., Onorato, R. M., Saykally, R. J., Liphardt, J., and Yang, P. D., "Tunable nanowire nonlinear optical probe," Nature 447, 1098-1101 (2007).
[21] Sandeau, N., Le Xuan, L., Chauvat, D., Zhou, C., Roch, J. F., and Brasselet, S., "Defocused imaging of second harmonic generation from a single nanocrystal," Opt. Express 15, 16051-16060 (2007).
[22] Delahaye, E., Tancrez, N., Yi, T., Ledoux, I., Zyss, J., Brasselet, S., and Clement, R., "Second harmonic generation from individual hybrid MnPS3-based nanoparticles investigated by nonlinear microscopy," Chem. Phys. Lett. 429, 533-537 (2006).
[23] Konig, K., So, P. T. C., Mantulin, W. W., and Gratton, E., "Cellular response to near-infrared femtosecond laser pulses in two-photon microscopes," Opt. Lett. 22, 135-136 (1997).
[24] Pu, Y., and Meng, H., "Intrinsic speckle noise in off-axis particle holography," J. Opt. Soc. Am. A-Opt. Image Sci. Vis. 21, 1221-1230 (2004).
[25] Lorenz, M. R., Holzapfel, V., Musyanovych, A., Nothelfer, K., Walther, P., Frank, H., Landfester, K., Schrezenmeier, H., and Mailander, V., "Uptake of functionalized, fluorescent-labeled polymeric particles in different cell lines and stem cells," Biomaterials 27, 2820-2828 (2006).
[26] Centurion, M., Pu, Y., and Psaltis, D., "Holographic capture of femtosecond pulse propagation," J. Appl. Phys. 100, 063104 (2006).